Summary: The formation of finite-sized microgel particles was revealed by photon correlation spectroscopy in aqueous solutions of hydrophobically associative polyelectrolyte polystyrene-*block*-poly(sodium methacrylate)-*block*-polystyrene. Starting from the lowest polymer concentration (1×10^{-6} g · L^{-1}) up to 1 g · L^{-1} a single relaxation process dominates the spectrum of relaxation times of the polymer solutions. This dominant mode was attributed to the diffusive motion of supramolecular microgel particles with a size of about 100 nm. Above a polyelectrolyte concentration of 1.0 g · L^{-1}, the size of the microgel grows up to ca. 300 nm. At a polymer concentration 20 g · L^{-1}, macroscopic phase separation occurs: the liquid phase of the microgel-cluster solution coexists with the phase of the macroscopic gel.

Schematic representation of the formation of supramolecular structures in aqueous solutions of hydrophobically associative polyelectrolyte.
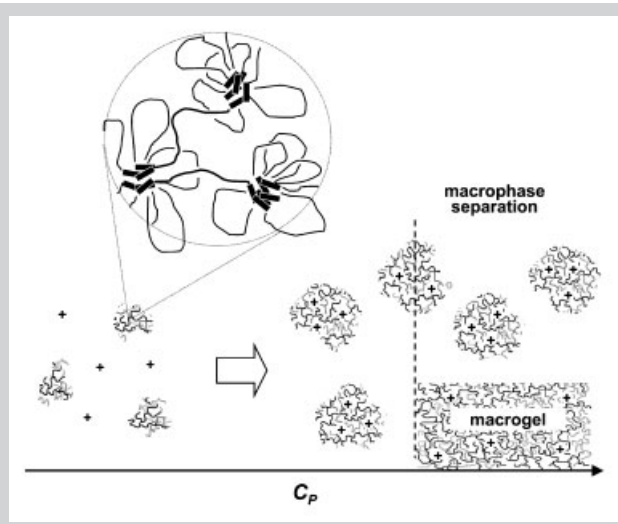
Clusters of Optimum Size Formed by Hydrophobically Associating Polyelectrolyte in Homogeneous Solutions and in Supernatant Phase in Equilibrium with Macroscopic Physical Gel

This paper is dedicated to Professor *Gerhard Wegner* with respect to his outstanding contribution to the field of polymer science and on the occasion of his 65th birthday

Yuri D. Zaroslov,[1] *Georgios Fytas,*[2,3] *Marinos Pitsikalis,*[4] *Nikos Hadjichristidis,*[4] *Olga E. Philippova,*[1] *Alexei R. Khokhlov*[1]

[1] Physics Department, Moscow State University, Leninskie Gory, 119992 Moscow, Russia
 Fax: 007(095)939-29-88; E-mail: zaroslov@polly.phys.msu.ru
[2] Institute of Electronic Structure and Laser, F.O.R.T.H., P.O. Box 1527, 71110 Heraklion, Crete, Greece
[3] Max Planck Institute for Polymer Research, P.O. Box 3148, 55021 Mainz, Germany
[4] Chemistry Department, University of Athens, Panepistimiopolis, Zografou 157 71, Greece

Introduction

Water-soluble associative polymers have attracted great attention during recent years. These objects are interesting both for researchers and engineers. One reason for this is a diversity of practical applications of these systems. Ecologically friendly water-based technologies are used in medicine, food industry, cosmetics, oil recovery, coatings, etc. The special place among associative polymers belongs to associative polyelectrolytes, which comprise a diversity of natural polymers, playing a vital role in living systems.

Despite the fact that associative polymers have been explored both experimentally and theoretically for several decades,[1−7] limited work has been done so far to describe the phase behavior of aqueous solutions of associative polyelectrolytes. A theoretical approach to the problem was undertaken recently for end-capped polyelectrolytes by two associative groups.[8] One of the original and most

interesting predictions of the theory is the existence of an equilibrium phase of microgel clusters formed by associative polyelectrolytes in aqueous solution. Inside the microgel different polymer chains form a network where the intermolecular aggregates of the sticker groups play the role of cross-linkers. The size of the clusters is determined by the interplay of opposing effects. While the increase of association energy of the sticker groups of the polymer makes the physical cross-links more stable and favors the growth of the aggregates, electrostatic repulsion of the charged groups of the polymer chains and translational entropy of mobile counter-ions counteracts the growth. Upon the increase of polymer concentration a macroscopic gel phase appears in coexistence with a supernatant phase of microgels. Addition of polymer to the system at this stage causes the growth of the macroscopic gel phase until it occupies the whole volume of the system.

Meanwhile, no unambiguous evidence of the existence of such microgels in aqueous solutions of associative polyelectrolytes has been obtained experimentally. In some cases, in dilute aqueous solutions of hydrophobically modified polyelectrolytes, the particles of several tens of nm in size were observed.[9−11] Nevertheless, the identification of these particles with the microgel clusters of finite size is still not clear. In addition, no experimental data indicating the existence of supramolecular aggregates in supernatant phase in macrophase-separated solutions of associative polyelectrolytes are available.

The present study of the association behavior of model polyelectrolytes in aqueous media was undertaken in order to cover the lack of systematic investigation of the phase behavior of associative polyelectrolytes in solutions. In particular, the existence of microgel clusters of finite size was of primary interest for us. A polystyrene-*block*-poly-(sodium methacrylate)-*block*-polystyrene ((PS)₂PMANa) copolymer synthesized by anionic polymerization was used as an associative polyelectrolyte. The polystyrene terminal blocks undergo hydrophobic association in aqueous media playing the role of the sticker groups, while the dissociation of the sodium acrylate units ensures a poly-

electrolyte character of the intermediate block. The well-defined structure of the polymer (known lengths of the blocks, narrow molecular weight distribution) makes it very promising as a model substance. In this paper the results of a structural and dynamic study by means of photon correlation spectroscopy of aqueous solutions of this polymer are presented.

Experimental Part

Synthesis and Characterization of the Model Triblock Copolymer

The sample was prepared by anionic polymerization using high vacuum techniques. The monomers (styrene, S, *tert*-butyl methacrylate, *tert*-BuMA and 1,1-diphenylethylene, DPE) and the solvent (tetrahydrofuran, THF) were purified according to well-established procedures.[12] The initiator, *s*-BuLi was prepared by the reaction of *s*-BuCl with Li under vacuum. S (10.2 g) was polymerized first in THF at $-78\,°C$ using *s*-BuLi $(2.75 \times 10^{-4}$ mol) as initiator. After the completion of the polymerization a small amount of DPE was introduced (3:1 molar ratio for the living ends) followed by the addition of *tert*-BuMA (4.1 g), which was distilled into the reactor for the synthesis of the living polystyrene-*block*-poly(*tert*-butyl methacrylate) lithium salt (PS-*b*-P*t*BuMA⁻Li⁺) diblock copolymer. The living polymer was then reacted with 1,4-di(bromomethyl)benzene $(1.30 \times 10^{-4}$ mol) to form the triblock copolymer PS-*b*-P*t*BuMA-*b*-PS as illustrated in Scheme 1. It has been previously shown that (bromomethyl)benzene derivatives can be efficiently used as linking agents for poly-methacrylate chains.[13,14] The linking reaction was allowed to take place at $-78\,°C$ for 24 h. Heat-sealing samples from the reactor of the PS block or the PS-*b*-PtBuMA diblock copolymer is not possible, because of the pyrolysis of THF, which will form by-products that will terminate the living polymer chains. Therefore, the final product of the linking reaction was analyzed by size exclusion chromatography (SEC), as shown in Figure 1. The excess diblock copolymer was removed by fractionation using toluene/heptane as the solvent/non-solvent system. The pure product was finally precipitated in heptane and was dried under vacuum for several days.
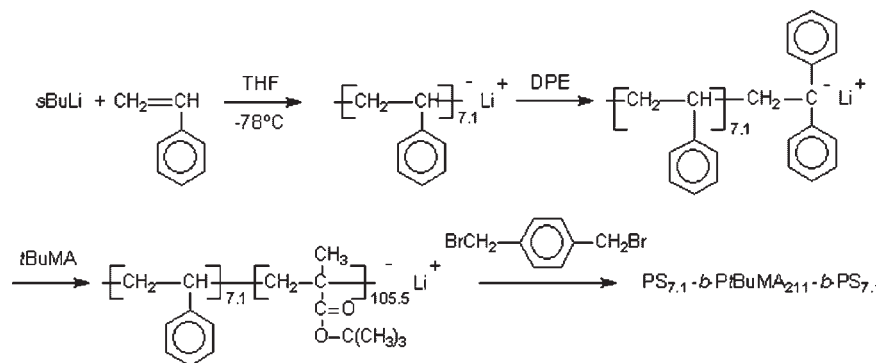
Scheme 1. Synthesis of polystyrene-*block*-poly(*tert*-butyl methacrylate)-*block*-polystyrene triblock copolymer.

Clusters of Optimum Size Formed by Hydrophobically Associating Polyelectrolyte in Homogeneous Solutions . . .

**Macromolecular
Chemistry and Physics**   175
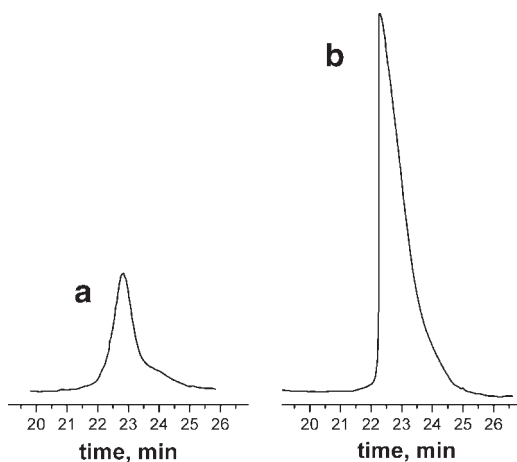
Figure 1. SEC chromatogram of the $PS_{7.1}$-b-$PtBuMA_{211}$-b-$PS_{7.1}$ triblock copolymer in THF at $40\,°C$: a) crude product, b) fractionated sample.

The sample was characterized by SEC and membrane osmometry. SEC experiments were conducted at $40\,°C$ using a modular instrument consisting of a Waters Model 510 pump, a Waters Model U6K sample injector, a Waters Model 401 differential refractometer, a Waters Model 486 UV spectrophotometer, and a set of four m-Styragel columns with a continuous porosity range from 10^6 to 10^3 Å. The columns were housed in an oven thermostated at $40\,°C$. THF was the carrier solvent at a flow rate of $1\ mL \cdot min^{-1}$. A Jupiter Model 231 membrane osmometer was used for the determination of the number-average molecular weight, $\bar{M}_n$ at $35\,°C$. Toluene distilled over CaH_2 was the solvent, whereas cellulose acetate membranes, purchased by Jupiter Instruments Co. were employed. The molecular weight distribution of the sample from the SEC analysis was 1.06 and the number-average molecular weight, $\bar{M}_n$ by MO was 31 400. According to ^1H NMR spectroscopy the triblock copolymer contains 4.6 wt.-% PS meaning that each of the end PS blocks has an average degree of polymerization equal to 7.1 and the PtBuMA middle block is equal to 211, $PS_{7.1}$-b-$PtBuMA_{211}$-b-$PS_{7.1}$. The $tert$-butyl groups were subsequently hydrolyzed using aqueous $6\ N$ HCl in dioxane at $85\,°C$ for 5 h.[15] ^1H NMR analysis (Varian Unity Plus 300/54) using $(D_6)DMSO$ as the solvent revealed the complete hydrolysis of the $tert$-butyl groups.

Preparation of Polymer Solutions

In its initial state with hydrophilic units in the acidic form, the polymer under study is not soluble in water. For the preparation of aqueous solutions, the polymer was dissolved in the presence of sodium hydroxide sufficient for a complete neutralization of its acidic groups. The dissolution took place under continuous stirring at $60\,°C$ for one day and the obtained solutions were left for equilibration at ambient temperature. Before measurements samples were left to equilibrate at room temperature without stirring for at least 3 d. Solutions with polymer concentrations below $1\ g \cdot L^{-1}$ (stock solution) were prepared by consecutive dilutions as follows: a few mL of the stock solution were diluted 10 times and maintained at $60\,°C$

for 1 h under continuous stirring before the next dilution took place. The whole series of the samples were stirred for 24 h from the start of the preparation procedure at $60\,°C$ and then left for equilibration for at least 3 d. Prior to light scattering experiments the prepared polymer solutions were filtered through cellulose acetate Millpore membranes with a $0.45\ \mu m$ pore size.

Photon Correlation Spectroscopy

The intermediate scattering function $C(q,t) = [(G(q,t) - 1)/f^*]^{1/2}$ was computed from the measured auto-correlation function $G(q,t) = \langle I(q,t)I(q,0)\rangle / \langle I(q)\rangle^2$ of the light-scattering intensity recorded by an ALV-5000 full digital correlator at different wave vectors q over the broad time range 10^{-6}–10^3 s; f^* is a coherence instrumental factor. The light source was a Nd/YAG dye-pumped, air-cooled laser (Adlas DPY 325) with a single mode intensity of 100 mW at the wavelength $\lambda = 532$ nm. The scattering angle was varied between 20 and $150°$.

The analysis of $C(q,t)$ proceeded by the inverse Laplace transformation using a constrained regularized CONTIN method:

$$C(q,t) = \int L(\ln \tau) \exp(-t/\tau) \mathrm{d} \ln \tau \qquad (1)$$

assuming only a superposition of exponential functions. The distribution $L(\ln \tau)$ of relaxation times can exhibit more than one peak characterized by its position τ_i and the area α_i which define the relaxation rate $\Gamma_i(= 1/\tau_i)$ and the intensity $I_i(q) = \alpha_i q/I(q)$ with $I(q)$ being the total scattering intensity at a given q. The validity of the performed analysis was evidenced by consistent and physically meaningful q-dependencies for the intensity and rate of the contributing modes to the experimental relaxation function.[16]

Results and Discussion

Homogeneous Solutions of Associative Polyelectrolyte

Aqueous solutions of $(PS)_2PMANa$ copolymer over the concentration range 1×10^{-6} to $20\ g \cdot L^{-1}$ were studied by photon correlation spectroscopy (PCS). The field correlation functions $C(q,t)$ together with distribution functions $L(\ln \tau)$ are presented in Figure 2. It is seen that for concentrations below $10\ g \cdot L^{-1}$, the relaxation distribution function $L(\ln \tau)$ is dominated by a single process.

The scattering intensity I_1 and relaxation rate Γ_1 associated with the main relaxation process are shown in Figure 3a and 3b as a function of q^2 for $1 \times 10^{-4}\ g \cdot L^{-1}$ solution of $(PS)_2PMANa$. It is seen that the scattering intensity $I_1(q)$ drastically changes with q (Figure 3a). The interpretation of these data depends on the underlying scattering mechanism. In principle, both pretransitional strong concentration fluctuations and supramolecular assemblies can lead to the behavior displayed in Figure 3. However, the present dilute solution is far from any phase boundary and the relaxation
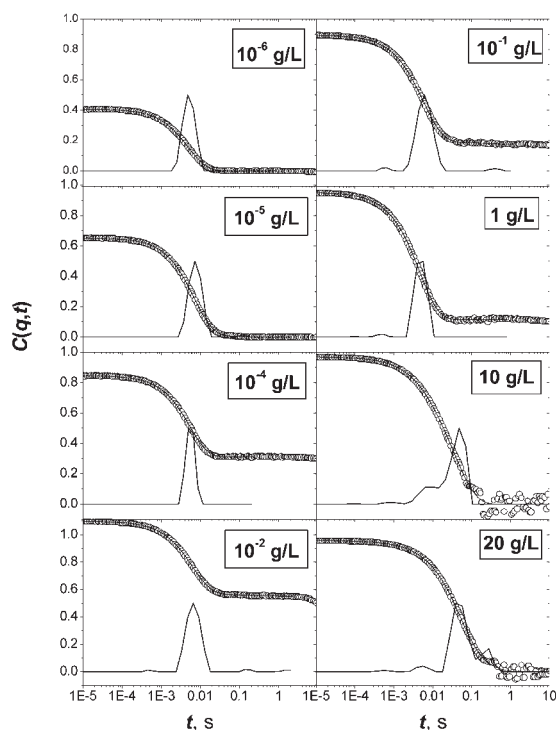
Figure 2. Field correlation function and inverse Laplace transform performed by CONTIN for an aqueous solution of (PS)$_2$PMANa at different polymer concentrations and a scattering angle of 30°. At a polymer concentration of 20 g·L^{-1} macroscopic phase separation occurs. The data presented in the figure for this polymer concentration were obtained by studying the light scattering of the supernatant liquid phase.

Figure 3. The variation of the intensity (a) and the rate (b) of the main relaxation process in 1×10^{-4} g·L^{-1} aqueous solution of (PS)$_2$PMANa with q^2 at 20 °C. Solid lines fit a linear dependence in the low q limit ($R \cdot q < 1$). Dashed vertical lines mark the inflexion point corresponding to $R \cdot q \approx 1$, where R is the overall size of the diffusing particles.

rate exhibits stronger than pure diffusive behavior, typical for near-critical thermodynamic fluctuations. Hence, we will discuss the data in terms of object-like supramolecular structures at dilute conditions.

To estimate the size of these objects we utilize the angular dependence of the scattering intensity corresponding to their translation diffusion (Figure 3a). The Debye theory of light scattering on the dilute solution of non-interacting particles predicts a linear dependence of the scattering intensity on q^2 at low $q \cdot R$:

$$I(q)\Big|_{Rq \ll 1} = I(0)\left(1 - \frac{R_g^2 q^2}{3}\right) \tag{2}$$

where R and R_g are the size of the particle and its radius of gyration. From the slope of the linear dependence at low q values ($R \cdot q < 1$) the radius of gyration R_g of the scattering particles is computed to be ca. 110 nm. The value of q ($\approx 1.2 \times 10^{-2}$ nm^{-1}) above which $I(q^2)$ deviation from Equation (2) is observed can be approximately related to the size of the particles as $R \approx 1/q$, which gives the value of R (≈ 80 nm) comparable to that of R_g. Both the value of the radius of gyration R_g and the estimation of the size of the scattering particles R are much larger then the estimated

size of the single triblock coil (ca. 7 nm), which implies that the scattering particles are supramolecular aggregates.

This large size of the scattering objects is also manifested in the high-absolute-reduced Rayleigh intensity $R(0)/C_p = K \cdot \overline{M}_w$, where $R(0) \propto I_1(0)$, K is the optical constant of the solution, and $\overline{M}_w$ is the weight-average molecular weight of the scattering particles. Using the refractive index contrast, $dn/dC_p = 0.17$ mL·g^{-1} [17] and $K = 4.2 \times 10^{-7}$ cm^2·mol·g^{-2}, $\overline{M}_w$ is estimated to be about 5×10^8 g·mol^{-1}. The reality of such a high value of molecular weight $\overline{M}_w$ can be checked by the calculation of the average polymer volume fraction inside the microgel particles $\phi = 3\overline{M}_w/(\rho_P N_A \cdot 4\pi R^3)$, where the density of the polymer ρ_P was taken to be about 1 g·mL^{-1} and the size of the microgels $R \approx 110$ nm (Figure 4). This calculation gives the value of $\phi \approx 0.15$, which is several times higher than the value of polymer volume fraction calculated for physical gels of polyelectrolyte telechelics in ref.,[8] but still quite below the upper physical limit of $\phi = 1$.

Complementary information on the structure of the particles can be obtained from the analysis of the relaxation rate Γ_1 in Figure 3b. A purely diffusive relaxation rate $\Gamma(q)$ ($\propto q^2$) is usually observed for particles with $q \cdot R \ll 1$, which applies in our case only for the lowest q values (vertical dashed line in the Figure 3b). The faster rate at high q results from the contribution of internal dynamics of the diffusing

Clusters of Optimum Size Formed by Hydrophobically Associating Polyelectrolyte in Homogeneous Solutions . . .

**Macromolecular
Chemistry and Physics** 177
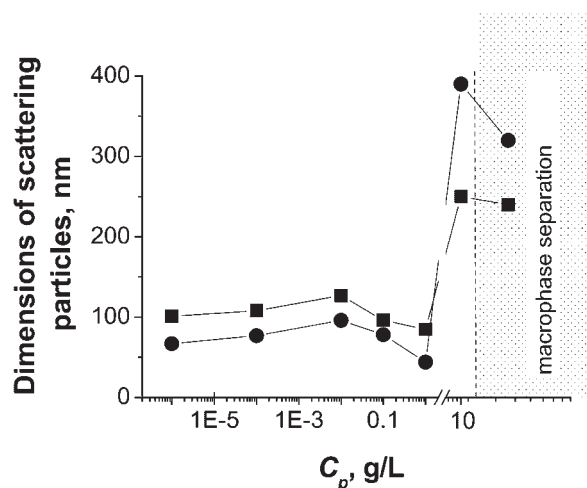
Figure 4. Estimation of the hydrodynamic radius R_h (circles) and the radius of gyration R_g (squares) of the scattering particles for different (PS)$_2$PMANa concentrations. The vertical dashed line marks the boundary between regions of the homogeneous state and macrophase separation (see text).

particles. The translational diffusion coefficient of the particles, D_0, is obtained as a low q limit of the effective diffusion coefficient $D_{eff} = \Gamma(q)/q^2$. Both the low value of $D_0 = 2.8 \times 10^{-8}$ cm$^2 \cdot$ s^{-1} and the strong q-dependent $I_1(q)$ corroborate the assumption that the scattering arises from supramolecular objects. The hydrodynamic radius R_h of these objects can be obtained from the Stokes-Einstein relation:

$$R_h = \frac{k_B T}{6\pi\eta_s D_0} \qquad (3)$$

where k_B and T are the Boltzmann constant and absolute temperature, and η_s the solvent viscosity. At $C_p = 1 \times 10^{-4}$ g$\cdot$L^{-1}, R_h amounts to ca. 80 nm. This value is in a good agreement with the value of q ($\approx$0.01 nm^{-1}) above which $\Gamma_1(q)$ deviates from a purely diffusive dependence. Hence, the analysis of the scattering intensity and rate dependencies on q gives comparable values for the hydrodynamic radius R_h, the radius of gyration R_g, and the size of the scattering particles R. The analysis of the PCS data for the other polymer concentrations yields similar results (Figure 4).

For (PS)$_2$PMANa concentrations above 0.01 g$\cdot$L^{-1}, aside from the main dominant process, the distribution L(ln τ) displays an additional weak peak at short relaxation times. The cooperative diffusion of mobile counter-ions and the polymer chains promoted by long-range electrostatic interactions can be responsible for the appearance of this fast relaxation mode. Alternatively, this mode can be interpreted as a manifestation of the diffusive motion of the single polymer chains or their micellar aggregates (see below). Unfortunately, the weak intensity of this fast relaxation process does not allow a reliable analysis of the data.

The dimension of the scattering particles retains its value of about 100 nm over a wide range of the polymer concentrations (from 1×10^{-6} to 1 g$\cdot$L), whereas the size of the particles increases up to 300 nm approaching the macrophase separation region.

An insight to the nature of the scattering objects can result from the comparison with the dimensions of the structures usually observed in solutions of telechelic polymers. From the available data in the literature, polymers end-capped by associative groups exist in selective solvents in the form of single chains and/or flower-like micelles.[18–21] As was mentioned above, an estimate of the size of a single coil (PS)$_2$PMANa is about 7 nm. The upper boundary for the flower-like micelle radius is 30 nm, which corresponds to a fully stretched hydrophilic part of the (PS)$_2$PMANa molecule in the corona. Both the single chains (7 nm) and the flower-like micelles (30 nm) are clearly smaller than the objects probed by PCS in (PS)$_2$PMANa aqueous solutions (100 nm). Hence, the microgels proposed by Potemkin et al.[8] or multi-core micelles proposed by Noda and Morishima[9] are better approximations of the structure of (PS)$_2$PMANa in aqueous solutions. The internal structure of the microgel clusters can be proposed as a network of flower-like micelles interconnected by bridging chains (Figure 5).

At low polymer concentrations (from 1×10^{-6} to 1 g$\cdot$L^{-1}) the size of the microgels is about 100 nm with the hydrodynamic radius R_h being less than R_g, which implies diffusion of rather loose particles drained by the solvent or objects with uneven or anisotropic shape. An increase of the polymer concentration above 1 g$\cdot$L^{-1} is characterized by the growth of the aggregates up to 300 nm and by the change of the relation between hydrodynamic R_h and gyration R_g radii. Above 1 g$\cdot$L^{-1}, the hydrodynamic
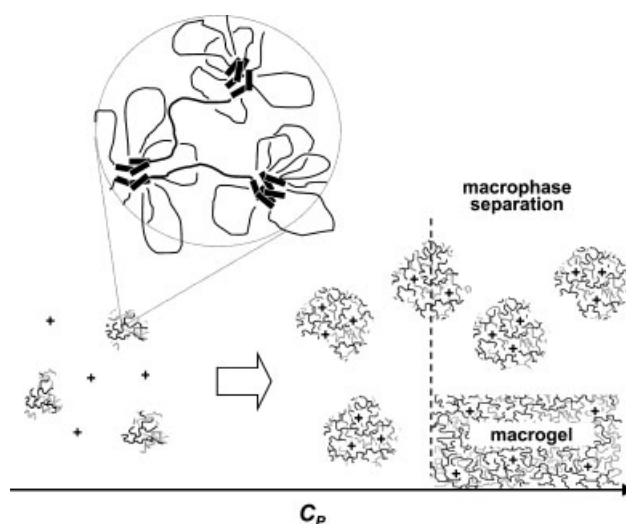
Figure 5. Schematic representation of the formation of supramolecular structures in aqueous solutions of telechelic polyelectrolyte (see text).

radius R_h becomes larger than R_g, which corresponds to the diffusion of compact objects (Figure 4).

According to ref.,[8] the optimum size of a microgel is determined by the balance of association energy favoring growth, and electrostatic repulsion together with translation entropy of counter-ions counteracting the growth. At low polymer concentrations, the entropy of mobile counter-ions in the outer solution dominates and the major fraction of counter-ions escapes from the aggregates, which become charged. The positive energy of electrostatic interaction of noncompensated charges of the microgels constrains their growth. An increase of polymer concentration (or concentration of microgels in solution) suppresses the counter-ions entropy. Nevertheless, the size of the microgels remains constant, until the contribution of the translational entropy of counter-ions becomes comparable with the energy of electrostatic repulsion. Then, the fraction of counter-ions trapped inside the aggregates increases; microgels grow and become more compact (Figure 4 and 5). Hence, the evolution of the size and shape of the observed microgels with the increase of associative polyelectrolyte concentration can be qualitatively realized in terms of the model of finite-sized clusters.

Macroscopic Phase Separation

At high polyelectrolyte concentrations (20 g·L^{-1}) a macroscopic phase separation is observed. Centrifugation of the polymer solution at 20 g·L^{-1} speeds up the separation into a supernatant liquid phase and a precipitant phase of a macroscopic physical gel allowing for a PCS experiment for both the phases. The intermediate scattering functions of the two phases along with the relaxation distribution functions $L(\ln \tau)$ are shown in Figure 6. For comparison, Figure 6a displays the same quantities for the 10 g·L^{-1} homogeneous solution. The low contrast of $C(q,t)$ in the gel phase is an indication of a non-ergodic behavior and hence the two peaks of $L(\ln \tau)$ at long times depend on the probed volume.

The multimode spectra of relaxation times observed for two liquid phases (Figure 6a,b) can be a manifestation of the polydispersity of scattering particles. Nevertheless, three relaxation processes obtained for a polymer concentration of 10 g·L^{-1} (Figure 6a) and supernatant phase at 20 g·L^{-1} were resolved with quite good reproducibility over a wide q-range (from 5×10^{-3} to 2.5×10^{-3} nm^{-1}). The rates of both fast modes followed purely diffusive dependence. At the same time q^2 dependences of the relaxation rate and scattering intensity of the slowest process qualitatively resemble those observed for lower polymer concentrations (Figure 3). All these observations allow us to exclude the effect of polydispersity on the structure of relaxation spectra for high polymer concentrations (10 and 20 g·L^{-1}) and to apply the approach described above for analysis of the data obtained for these high polymer concentrations.
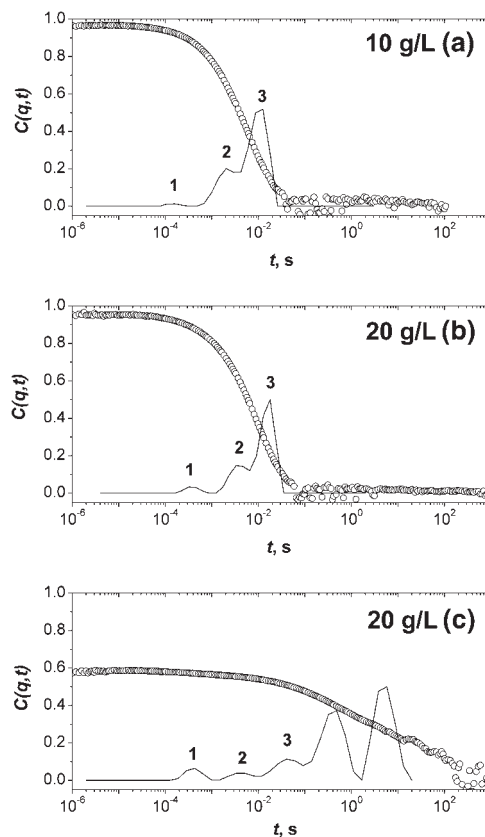
Figure 6. Intermediate scattering functions (circles) along with the distribution $L(\ln \tau)$ Equation (1) (solid lines) of two aqueous solutions of (PS)$_2$PMANa: (a) homogeneous solution at 10 g·L^{-1}; (b) supernatant homogeneous phase; and (c) macroscopic gel phase at 20 g·L^{-1}. The numbered relaxation modes are discussed in the text.

The scattering functions for the homogeneous 10 g·L^{-1} (Figure 6) and phase-separated solution in the supernatant phase (Figure 6b) look alike. Two fast relaxation modes, slightly slowed down, can also be resolved in the $L(\ln \tau)$ of the gel phase (Figure 6c). To compare the rates of these relaxation modes the apparent diffusion coefficients D_0 were calculated. The obtained values are listed in Table 1.

These results can be rationalized within the framework of the model of macroscopic phase separation presented in ref.[8] The phase coexistence for $C_p > 10$ g·L^{-1} can be identified with the microgel (supernatant) solution and the macroscopic gel (lower) phase. The closeness of the rates of modes 1 and 2 in all three cases (Figure 6 and Table 1) is evidence of the identity of fast dynamics in both the finite gel clusters and the percolated macroscopic gel. Slightly lower values of the apparent diffusion coefficients for modes 1 and 2 in the bulk of the macroscopic network (Table 1) can be related to the screening of electrostatic interactions and suppression of the mobility of polymer chains in this phase. The relaxation mode 3 in 10 g·L^{-1}

Clusters of Optimum Size Formed by Hydrophobically Associating Polyelectrolyte in Homogeneous Solutions . . .

**Macromolecular
Chemistry and Physics**   179

Table 1. The apparent diffusion coefficients D_0 calculated for the different relaxation modes for $10 \text{ g} \cdot \text{L}^{-1}$ $(PS)_2$PMANa solution, and for supernatant and gel phases at the average $(PS)_2$PMANa concentration of $20 \text{ g} \cdot \text{L}^{-1}$.

Number of mode (Figure 6)	Apparent diffusion coefficient D_0		
	$10^{-8} \text{ cm}^2 \cdot \text{s}^{-1}$		
	$10 \text{ g} \cdot \text{L}^{-1}$	$20 \text{ g} \cdot \text{L}^{-1}$ (supernatant phase)	$20 \text{ g} \cdot \text{L}^{-1}$ (gel phase)
1	32 ± 6	32 ± 5	18 ± 4
2	2.8 ± 0.4	2.5 ± 0.25	2.0 ± 0.4
3	0.224 ± 0.002	0.268 ± 0.026	0.091 ± 0.002

$(PS)_2$PMANa solution and in the supernatant phase at $20 \text{ g} \cdot \text{L}^{-1}$ solution can be attributed to the translational diffusive motion of microgel particles, which allows us to calculate the dimensions of the particles. Both hydrodynamic R_h and gyration R_g radii give values of about 300 nm (Figure 4). The coincidence within the experimental error of the microgels dimensions in the homogeneous solution at $10 \text{ g} \cdot \text{L}^{-1}$ (Figure 6a) and in the supernatant phase at $20 \text{ g} \cdot \text{L}^{-1}$ (Figure 6b) indicates that the observed macrophase separation is a truly equilibrium state. If this is the case, the size of the microgels should not change as soon as the new phase of the macroscopic gel is formed in the system upon increase of the polymer concentration. In the region of macrophase separation, the addition of the polymer to the system, therefore, leads to the growth of the volume occupied by the macrogel phase, while the size and concentration of the microgels in the supernatant phase remains constant. Hence, we can conclude that the polymer solution at a concentration of $10 \text{ g} \cdot \text{L}^{-1}$ falls into a pretransitional region followed by a macrophase separation, where the macroscopic physical gel coexists with a homogeneous solution of microgel clusters at polymer concentrations above $20 \text{ g} \cdot \text{L}^{-1}$.

Conclusion

The formation of supramolecular structures was revealed in aqueous solutions of the associative polyelectrolyte polystyrene-*block*-poly(sodium methacrylate)-*block*-polystyrene by photon correlation spectroscopy. The observed particles have a size of about 100 nm over a wide range of the polymer concentrations (from 1×10^{-6} to $1 \text{ g} \cdot \text{L}^{-1}$), they then increase in size up to 300 nm approaching the macrophase separation region. At about $20 \text{ g} \cdot \text{L}^{-1}$ macroscopic phase separation occurs: a macroscopic physical gel coexists with the solution of supramolecular clusters. The obtained data are discussed in terms of a model of finite-sized microgel clusters.[8] A good qualitative agreement of the theoretical predictions with experimental observations is demonstrated.

[1] "*Biological and Synthetic Polymer Networks*", O. Kramer, Ed., Elsevier, New York 1988.
[2] "*Polymers in Aqueous Media: Performance trough association*", J. E. Glass, Ed., Advances in Chemistry Series, Vol. 223, American Chemical Society, Washington, DC 1989.
[3] M. S. Green, A. V. Tobolsky, *J. Chem. Phys.* **1946**, *14*, 80.
[4] A. Coniglio, H. E. Stanley, W. Klein, *Phys. Rev. B* **1982**, *25*, 6805.
[5] F. Tanaka, W. H. Stockmayer, *Macromolecules* **1994**, *27*, 3943.
[6] A. N. Semenov, M. Rubinstein, *Macromolecules* **1998**, *31*, 1373.
[7] A. V. Ermoshkin, I. Ya. Erukhimovich, *J. Chem. Phys.* **1999**, *110*, 1781.
[8] I. I. Potemkin, V. V. Vasilevskaya, A. R. Khokhlov, *J. Chem. Phys.* **1999**, *111*, 2809.
[9] T. Noda, Y. Morishima, *Macromolecules* **1999**, *32*, 4631.
[10] T. Noda, A. Hashidzume, Y. Morishima, *Macromolecules* **2000**, *33*, 3694.
[11] T. Noda, A. Hashidzume, Y. Morishima, *Macromolecules* **2001**, *34*, 1308.
[12] N. Hadjichristidis, H. Iatrou, S. Pispas, M. Pitsikalis, *J. Polym. Sci., Part A: Polym. Chem.* **2000**, *38*, 3211.
[13] M. Pitsikalis, S. Sioula, S. Pispas, N. Hadjichristidis, D. C. Cook, J. Li, J. W. Mays, *J. Polym. Sci., Part A: Polym. Chem.* **1999**, *37*, 4337.
[14] N. Hadjichristidis, S. Pispas, H. Iatrou, M. Pitsikalis, *Curr. Org. Chem.* **2002**, *6*, 155.
[15] C. Ramireddy, Z. Tuzar, K. Prochazka, S. E. Webber, P. Munk, *Macromolecules* **1992**, *25*, 2541.
[16] A. Aggeli, G. Fytas, D. Vlassopoulos, T. C. B. McLeish, P. J. Mawer, N. Boden, *Biomacromolecules* **2001**, *2*, 378.
[17] K. Khougaz, I. Astafieva, A. Eisenberg, *Macromolecules* **1995**, *28*, 7135.
[18] A. Yekta, B. Xu, J. Duhamel, H. Adiwidjaja, M. Winnik, *Macromolecules* **1995**, *28*, 956.
[19] Y. Serero, R. Aznar, G. Porte, J. Berret, D. Calvet, A. Collet, M. Vaguier, *Phys. Rev. Lett.* **1998**, *81*, 5584.
[20] Q. T. Pham, W. B. Russel, J. C. Thibeault, W. Lau, *Macromolecules* **1999**, *32*, 2996.
[21] F. Lafleche, D. Durand, T. Nicolai, *Macromolecules* **2003**, *36*, 1331.